J. Phys. D: Appl. Phys. **40** (2007) 5130–5139 doi:10.1088/0022-3727/40/17/019

Sub-Alfvenic inlet boundary conditions for axisymmetric MHD nozzles

J T Cassibry[1] **and S T Wu**[2]

[1] Propulsion Research Center, University of Alabama in Huntsville, Huntsville, AL 35899, USA
[2] Center for Space Plasma and Aeronomy Research, University of Alabama in Huntsville, Huntsville, AL 35899, USA

E-mail: cassibj@uah.edu and wus@cspar.uah.edu

Received 27 February 2007, in final form 17 July 2007
Published 16 August 2007
Online at stacks.iop.org/JPhysD/40/5130

Abstract
There are numerous electromagnetic accelerator concepts which require plasma expansion through a magnetic nozzle. If the inlet flow is slower than one or all of the outgoing characteristics, namely, the Alfven, slow and fast magnetosonic speeds, then the number of inlet conditions which could be arbitrarily specified are reduced by the number of outgoing characteristics (up to three). We derive the axisymmetric compatibility equations using the method of projected characteristics for the inlet conditions in the z-plane to assure the boundary conditions being consistent with flow properties. We make simplifications to the equations assuming that the inlet Alfven speed is much faster than the sonic and slow magnetosonic speeds. We compare results for various inlet boundary conditions, including a modified Lax–Wendroff implementation of the compatibility equations, first order extrapolation and arbitrarily specifying the inlet conditions, in order to assess the stability and accuracy of various approaches.

(Some figures in this article are in colour only in the electronic version)

Nomenclature

$\boldsymbol{A}$	matrix of coefficients for partial derivative with respect to r for $\boldsymbol{W}$.
a	sound speed ($\mathrm{m\,s^{-1}}$)
B	magnetic induction field (T)
$\boldsymbol{C}$	matrix of coefficients for partial derivative with respect to z for $\boldsymbol{W}$.
c_v	specific heat ($\mathrm{J\,kg^{-1}\,K^{-1}}$)
f, g	generic functions
J	current density ($\mathrm{A\,m^{-2}}$)
k	Boltzmann's constant ($\mathrm{J\,K^{-1}}$)
m	mass (kg)
n	number density ($\mathrm{m^{-3}}$)
P	pressure ($\mathrm{N\,m^{-2}}$)
q	charge (C)
R	gas constant ($\mathrm{J\,kg^{-1}\,K^{-1}}$)
r	radial coordinate
s	general curve coordinate
$\boldsymbol{S}$	source term vector for MHD equation
T	temperature (K)
t	time (s)
u	velocity in x-direction ($\mathrm{m\,s^{-1}}$)
v	velocity ($\mathrm{m\,s^{-1}}$)
v_A	Alfvén speed ($\mathrm{m\,s^{-1}}$)
$v_{f,s}$	fast, slow magnetosonic speed ($\mathrm{m\,s^{-1}}$)
$\boldsymbol{W}$	primitive variable vector
x	one-dimensional coordinate (m)
z	axial direction
α	magnetic nozzle wall angle
ε	specific internal energy ($\mathrm{J\,kg^{-1}}$)
Φ	volume specific radiative power ($\mathrm{W\,m^{-3}}$)
γ	specific heat ratio
η	electrical resistivity ($\Omega\,\mathrm{m}$)
κ	thermal conductivity ($\mathrm{W\,m^{-1}\,K^{-1}}$)
$\lambda^{(j)}$	eigenvalues
μ_0	magnetic permeability of free space ($\mathrm{kg\,m\,C^{-2}}$)
$\xi^{(j)}$	left eigenvectors
ρ	density ($\mathrm{kg\,m^{-3}}$)
τ	collision time (s)

Subscripts

e	electron
eR	electron radiation
i	ion
r	radial coordinate
z	axial direction
θ	azimuthal direction

1. Introduction

Magnetic nozzles are intended to accelerate plasma along an applied magnetic induction field to create a directed plasma flow that detaches from a spacecraft to produce thrust [1]. A commonly expressed concern is that the on-board coils create magnetic fields with closed field lines. The question then arises of how the magnetically guided plasma can detach from the spacecraft, since the field lines close on the vehicle.

Several approaches have been considered to accomplish detachment, including recombination and charge exchange. However, recombination is very difficult to implement because the reaction rates are relatively slow. If neutral particles are injected into the flow to facilitate charge exchange/recombination, the fuel efficiency will drop precipitously.

A promising alternative scenario is that the outgoing plasma stretches the magnetic field lines along the flow and thereby detaches from the spacecraft together with the magnetic field [2]. This scenario is similar to what occurs in the solar wind and it is particularly relevant to high-power thrusters. It requires that the velocity of the plasma flow exceeds the Alfven velocity. It has been shown that ideal magnetohydrodynamic (MHD) theory predicts that a properly designed magnetic nozzle can gradually reduce the guiding magnetic field, so that the flow becomes highly super-Alfvenic and leaves the nozzle as a well-directed jet [2]. Since the theory has yet to be conclusively validated by experimental data, it would be beneficial to verify against computational MHD studies which can be extended to include nonideal effects and complex geometries. One of the principal challenges to appropriately developing such a computational tool is the appropriate specification of inlet boundary conditions.

Previous studies of magnetic nozzle perfomance and detachment have used either particle or fluid approaches. Kaufman *et al* [3] showed that collisionless separation can occur since finite electron mass suppresses azimuthal currents in the nozzle. Hooper identified a 2nd order cross-field drift [4] which is orthogonal to the nozzle field lines, but significant detachment may require dissipative effects.

Ilin *et al* [5] extended the detachment work to computer simulations using both particle and MHD techniques. Reasonable agreement was reached between the MHD and particle models in the detachment analysis. York *et al* [6] developed a single fluid 2D MHD code including all flow and dissipative effects. They were able to predict axial variations of properties in the corresponding experiments when a radial parabolic profile of electron density was specified, and found that electrical resistivity behaved classically.

Magnetic nozzle modelling efforts using MHD have not yet taken into consideration the compatibility relations for sub-Alfvenic inlet conditions, which may be important for accurate prediction of downstream conditions and computational stability. In this particular study, the flow regions cover from subsonic, sub-Alfvenic to supersonic, super-Alfvenic flow. Thus, the number of boundary conditions which could be specified depend on the characteristics. Specifically, when inlet flow speed is less than the slow magnetosonic speed, at least three of the inlet conditions should be computed based on the conditions in the computational domain. In this paper, we apply the method of projected characteristics [7–9] to determine the compatibility relations for two temperature axisymmetric MHD flow projected on the z–t plane. To the authors' knowledge, this is the first time the method of projected characteristics has been applied in this coordinate system. We then simplify the relations and discuss the numerical implementation. We then model a simple magnetic nozzle geometry and make some preliminary comparisons between three cases using different boundary conditions: (1) computational boundary conditions based on the derived compatibility equations, (2) extrapolation of three inlet parameters from the domain and (3) all parameters specified (no computed parameters).

2. Basic idea of method of characteristics

The method of projected characteristics was developed originally by Nakagawa [7]. Several good sources exist which discuss the technique including Nakagawa *et al* [8] and Wu and Wang [9]. For completeness, we discuss the basic idea of the method of projected characteristics, following previous authors.

2.1. Approach

A partial differential equation of a function $f(x,t)$ of two independent variables x and t,

$$\frac{\partial f}{\partial t} + u\frac{\partial f}{\partial x} = g, \tag{1}$$

can be written as a total differential equation of the form

$$\frac{\mathrm{d}f}{\mathrm{d}s} = g. \tag{2}$$

This transformation is possible as the definition of the directional derivative in the (x,t) plane along a curve $s(x,t)$ is

$$\frac{\mathrm{d}f}{\mathrm{d}s} = \frac{\partial f}{\partial t}\frac{\partial t}{\partial s} + \frac{\partial f}{\partial x}\frac{\partial x}{\partial s}, \tag{3}$$

where the direction of the curve $s(x,t)$ is

$$\frac{\mathrm{d}x}{\mathrm{d}t} = -\frac{\partial s/\partial t}{\partial s/\partial x} = u. \tag{4}$$

Thus, the solution of equation (1) can be obtained by integrating equation (2) along the curve $s(x,t)$ even for the nonlinear case of u *and* g being general functions of x and t in the form

$$f(s) = f(0) + \int_0^s g\,\mathrm{d}s, \tag{5}$$

where $f(0)$ denotes the values of $f(x,t)$ at $s = 0$.

This is the basic idea of the method of characteristics to obtain the solutions of nonlinear hyperbolic partial differential equations. The curves along which total differential equations can be derived are called the characteristics, while the resultant equations are called the compatibility equations. Various physical variables correspond to the function $f(x,t)$. The compatibility equations can be obtained for combinations of physical variables along a number of characteristics, which become surfaces for two or three-dimensional problems. The method of characteristics results in complex differential equations for the MHD governing equations. For axisymmetric MHD flows, the derivation of the equations is presented in appendix A.

2.2. *Simplifications to compatibility equations*

Equation (A.16) is too complex for practical implementation into a computer model. In order to derive the simplified equations, we first neglect gradients and time derivatives in the orthogonal θ-vector terms

$$\left(\frac{\partial B_\theta}{\partial t}, \frac{\partial B_\theta}{\partial r}, \frac{\partial B_\theta}{\partial z}, \frac{\partial v_\theta}{\partial t}, \frac{\partial v_\theta}{\partial r}, \frac{\partial v_\theta}{\partial z} = 0\right).$$

We note that these terms must be reconsidered in the presence of strong rotation. Since the sound speed is roughly an order of magnitude slower than the characteristic Alfven (v_A) speed, we can make first order approximations to $v_{f,s}$. Provided that the radial and azimuthal components of the field are much smaller than the axial (z) component at the inlet boundary, $v_A \approx v_{Az} = v_A$. Neglecting the a^4 term in equation (A.13), the first order Taylor expansion of the inner square root term is $v_A^2 - a^2$. Thus, it can be shown that the fast and slow magnetosonic speeds reduce to the Alfven and sonic speeds, respectively. With these approximations, the characteristic equations become

$$\begin{aligned}
&\frac{\mathrm{d}z}{\mathrm{d}t} = v_z - v_{fz},\\
&\frac{B_z B_r}{\mu_0}\frac{\partial v_r}{\partial t} + \frac{B_r v_{fz}}{\mu_0}\frac{\partial B_r}{\partial t}\\
&\quad = \left(-\frac{B_z B_r}{\rho\mu_0}\frac{a^2}{\gamma}\right)\frac{\partial \rho}{\partial r} + \left(-\frac{B_z B_r}{\mu_0}v_r - v_{fz}\frac{B_\theta^2}{\mu_0}\right)\frac{\partial v_r}{\partial r}\\
&\quad + \left(-C_{ve}(\gamma-1)\frac{B_z B_r}{\mu_0}\right)\frac{\partial T_e}{\partial r}\\
&\quad + \left(-C_{vi}(\gamma-1)\frac{B_z B_r}{\mu_0}\right)\frac{\partial T_i}{\partial r}\\
&\quad + \left(-\frac{B_z B_r}{\mu_0^2}\frac{(-B_r - B_\theta - B_z)}{\rho} - \frac{B_r}{\mu_0}v_{fz}v_r\right)\frac{\partial B_r}{\partial r}\\
&\quad + \frac{B_z B_r^2}{\mu_0^2\rho}\frac{\partial B_z}{\partial r} - (v_z - v_{fz})\frac{B_z B_r}{\mu_0}\frac{\partial v_r}{\partial z},\\
&\quad - v_{fz}(v_z - v_{fz})\frac{B_r}{\mu_0}\frac{\partial B_r}{\partial z} - \frac{9v_{fz}}{r}\left(\frac{B_r^2 v_r}{\mu_0} + \frac{B_r B_\theta v_\theta}{\mu_0}\right),
\end{aligned} \tag{6}$$

$$\begin{aligned}
&\frac{\mathrm{d}z}{\mathrm{d}t} = v - v_{Az},\\
&\frac{\partial B_z}{\partial t} = -B_z\frac{\partial v_r}{\partial r} + B_r\frac{\partial v_z}{\partial r} - v_r\frac{\partial B_z}{\partial r}\\
&\quad + (v_{Az} - v_z)\frac{\partial B_z}{\partial z} - \frac{9v_r B_z}{r},
\end{aligned} \tag{7}$$

$$\begin{aligned}
&\frac{\mathrm{d}z}{\mathrm{d}t} = v_z - v_{sz},\\
&\frac{v_{sz}}{\gamma}(-v_A^2)\frac{\partial \rho}{\partial t} + \frac{B_z B_r}{\mu_0}\frac{\partial v_r}{\partial t} - \rho(-v_A^2)\frac{\partial v_z}{\partial t}\\
&\quad + \frac{\rho v_{sz}R_e}{a^2}(-v_A^2)\frac{\partial T_e}{\partial t} + \frac{\rho v_{sz}R_i}{a^2}(-v_A^2)\frac{\partial T_i}{\partial t}\\
&\quad + v_{sz}\frac{B_r}{\mu_0}\frac{\partial B_r}{\partial t} = +\left(-\frac{v_{sz}v_r}{\gamma}(-v_A^2) - \frac{B_z B_r}{\rho\mu_0}\frac{a^2}{\gamma}\right)\frac{\partial \rho}{\partial r}\\
&\quad + \left(-\rho v_{sz}(-v_A^2) - \frac{B_z B_r v_r}{\mu_0} - v_{sz}\frac{B_\theta^2}{\mu_0}\right)\frac{\partial v_r}{\partial r} + \rho v_r(-v_A^2)\frac{\partial v_z}{\partial r}\\
&\quad + \left(-C_{ve}(\gamma-1)\frac{B_z B_r}{\mu_0} - \frac{\rho v_r v_{sz}R_e}{a^2}(-v_A^2)\right)\frac{\partial T_e}{\partial r}\\
&\quad + \left(-C_{vi}(\gamma-1)\frac{B_z B_r}{\mu_0} - \frac{\rho v_r v_{sz}R_i(-v_A^2)}{a^2}\right)\frac{\partial T_i}{\partial r}\\
&\quad + \left(-\frac{B_z B_r(-B_r - B_\theta - B_z)}{\rho\mu_0^2} - v_{sz}v_r\frac{B_r}{\mu_0}\right)\frac{\partial B_r}{\partial r}\\
&\quad + \frac{B_z B_r^2}{\mu_0^2\rho}\frac{\partial B_z}{\partial r} - \frac{v_{sz}}{\gamma}(v_z - v_{sz})(-v_A^2)\frac{\partial \rho}{\partial z}\\
&\quad - (v_z - v_{sz})\frac{B_z B_r}{\mu_0}\frac{\partial v_r}{\partial z} + \rho(v_z - v_{sz})(-v_A^2)\frac{\partial v_z}{\partial z}\\
&\quad - \frac{\rho v_{sz}R_e}{a^2}(v_z - v_{sz})(-v_A^2)\frac{\partial T_e}{\partial z}\\
&\quad - \frac{\rho v_{sz}R_i}{a^2}(v_z - v_{sz})(-v_A^2)\frac{\partial T_i}{\partial z}\\
&\quad - v_{sz}(v_z - v_{sz})\frac{B_r}{\mu_0}\frac{\partial B_r}{\partial z}\\
&\quad - \frac{9v_{sz}}{r}\left(\frac{B_r^2 v_r}{\mu_0} + \frac{B_r B_\theta v_\theta}{\mu_0} + \frac{\rho v_r}{\gamma}(-v_A^2)\right)\\
&\quad - \frac{9\rho v_{sz}}{a^2}(-v_A^2)\left(\frac{(\gamma-1)v_r}{r}(R_e T_e + R_i T_i)\right.\\
&\quad \left. + \frac{(T_e - T_i)}{\tau_{ei}}(R_e - R_i)\right).
\end{aligned} \tag{8}$$

Since there are only three outgoing characteristics in the nozzle inlet provided the flow direction is into the nozzle, we can simplify equations (6)–(8) above by specifying the remaining variables and setting the corresponding time derivatives to zero, assuming constant inlet conditions. It is arbitrary which variables are chosen. Physically, it is advantageous to specify inlet mass flow rate and energy, so that inlet flow conditions match that of possible experiments. Thus, we can specify ρ, T_e, T_i, v_z, and use the compatibility relations for v_r, B_r and B_z. Setting the time derivatives for ρ, T_e, T_i and v_z to zero, subtracting equation (8) from equation (6), and using the ideal gas law $P = \rho(R_e T_e + R_i T_i)$, we have the much simpler

equation

$$\frac{B_r v_A}{\mu_0}\frac{\partial B_r}{\partial t} = -\frac{v_A^2 v_r}{a}\frac{\partial P}{\partial r} + \left(-\rho a v_A^2 - v_A\frac{B_\theta^2}{\mu_0}\right)\frac{\partial v_r}{\partial r} + \rho v_r v_A^2\frac{\partial v_z}{\partial r} - \frac{B_r}{\mu_0}v_A v_r\frac{\partial B_r}{\partial r} - (v_z - v_A)\frac{B_z B_r}{\mu_0}\frac{\partial v_r}{\partial z} + \rho v_A^2 (v_z - a)\frac{\partial v_z}{\partial z} - \frac{v_A^2}{a}(v_z - a)\frac{\partial P}{\partial z} - v_A (v_z - v_A)\frac{B_r}{\mu_0}\frac{\partial B_r}{\partial z} - \frac{9 v_A}{r}\left(\frac{B_r^2 v_r}{\mu_0} + \frac{B_r B_\theta v_\theta}{\mu_0} + \frac{P\gamma v_A v_r}{a} + \frac{\rho r v_A (T_e - T_i)(R_e - R_i)}{a\tau_{ei}}\right). \quad (9)$$

We can use equation (9) for the time derivative of B_r in equation (6). Using the ideal gas law and putting $\partial B_r/\partial t$ on the RHS, we have

$$\frac{B_z B_r}{\mu_0}\frac{\partial v_r}{\partial t} = -\frac{B_r v_A}{\mu_0}\frac{\partial B_r}{\partial t} - \frac{B_z B_r}{\rho\mu_0}\frac{\partial P}{\partial r} + \left(-\frac{B_z B_r}{\mu_0}v_r - v_A\frac{B_\theta^2}{\mu_0}\right)\frac{\partial v_r}{\partial r} + \left(-\frac{B_z B_r}{\mu_0^2}\frac{(-B_r - B_\theta - B_z)}{\rho} - \frac{B_r}{\mu_0}v_A v_r\right)\frac{\partial B_r}{\partial r} + \frac{B_z B_r^2}{\mu_0^2\rho}\frac{\partial B_z}{\partial r} - (v_z - v_A)\frac{B_z B_r}{\mu_0}\frac{\partial v_r}{\partial z} - v_A(v_z - v_A)\frac{B_r}{\mu_0}\frac{\partial B_r}{\partial z} - \frac{9 v_A}{r}\left(\frac{B_r^2 v_r}{\mu_0} + \frac{B_r B_\theta v_\theta}{\mu_0}\right). \quad (10)$$

For positive flow in the inlet, there are four different cases for inlet conditions. If $v < v_s$, then B_r, B_z and v_r must be determined from equations (7), (9) and (10). If $v_s < v < v_A$, then B_r and B_z are determined from equations (7) and (9) and v_r can be specified. If $v_A < v < v_f$, then equation (9) determines the evolution of B_r, and all other variables are specified. Finally, if the flow velocity is greater than all the characteristic waves, all variables can be specified arbitrarily.

2.3. Formulation

Equations (7) and (9) were programmed into the numerical model to advance radial and axial components of the magnetic field. We used a two step Lax–Wendroff second order scheme with 2nd order forward differencing of derivatives in the z direction and central differencing in the r direction. We field aligned the radial component of velocity at the inlet to eliminate $\boldsymbol{v}\times\boldsymbol{B}$ convection of the field at the inlet which might artificially induce azimuthal currents. This approach avoids the need to use equation (10). When B_r is small at the inlet, equation (9) will blow up. In order to avoid this when B_r is small ($<10^{-4}$ T in this model), B_r is then found using

$$B_{r_{i,0}} = \frac{1}{3r_{i,0}}\left(r_{i,0}\left(\frac{-3B_{z_{i,0}} + 4B_{z_{i,1}} - B_{z_{i,2}}}{\Delta z}\right)\Delta r + 4r_{i-1,0}B_{r_{i-1,0}} - r_{i-2,0}B_{z_{i-2,0}}\right), \quad (11)$$

which is the 2D solution to $\nabla\cdot B = 0$ in the r–z plane in cylindrical coordinates, using 2nd order backwind differencing in r and 2nd order forward differencing in z.

3. Numerical model

3.1. MHD solver

An axisymmetric MHD nozzle model was developed to support the diagnostic analysis and to enable rapid investigations of the effects of various input parameters related to nozzle geometry, applied magnetic field topology and upstream flow conditions. This tool was intended to allow optimization of magnetic nozzle design. MACH2 [10, 11], a $2\frac{1}{2}D$ multiblock, arbitrary Lagrangian Eulerian (ALE), resistive, single fluid MHD code was used to develop the model. MACH2 carries all three spatial components of vectors, but allows no quantity to depend on the coordinate that is normal to the computational plane. MACH2 solves the mass, momentum, electron energy, ion energy, radiation energy density and magnetic induction equations in a fractional time-split manner for the flow variables. The equations are closed with an ideal gas equation of state, Braginskii thermal conductivity for components perpendicular and parallel to the magnetic field and Spitzer resistivity. All computations were performed on a Dell Precision 360 workstation with a Pentium IV 3.6 GHZ CPU with 1 GB of RAM running Mandrake 9.1 linux.

3.2. Magnetic nozzle description

The motivation for deriving the axisymmetric compatibility relations was to correctly specify subsonic, sub-Alfvenic inlet boundary conditions for a magnetic nozzle. There is interest in using a nozzle in some electric propulsion devices. A current theory for practical application of such a device for in-space propulsion is to expand the plasma to super-Alfvenic flow within the nozzle to achieve detachment from the nozzle [2]. If the inlet plasma conditions and magnetic geometry are designed carefully, the plasma can transition to super-Alfvenic flow inside the nozzle. As the plasma expands outside the nozzle, the plasma will dictate the magnetic field, stretching field lines indefinitely and achieving 'detachment'. If the nozzle walls are flux conserving and the field strength is essentially uniform for all r at some position z, then the nozzle exit to inlet radius ratio criteria to permit super-Alfvenic detachment can be shown to be

$$\frac{r_{\text{exit}}}{r_{\text{inlet}}} \geqslant B_{\text{inlet}}\left(\frac{m}{2kT\rho\mu_0}\right)^{1/2}. \quad (12)$$

In order to properly develop an MHD nozzle model to test this criteria and to use the model to study nozzle performance, the conditions must satisfy some basic constraints. Firstly, the Larmor radius and collision mean free path must be smaller than the scale size of the device. Secondly, not all inlet conditions can be specified simultaneously, because by design, the inlet flow is sub-Alfvenic. This means that at least two or perhaps three plasma parameters must be computed based on interior conditions in the flow. Finally, due to the simplifications made in the compatibility equations

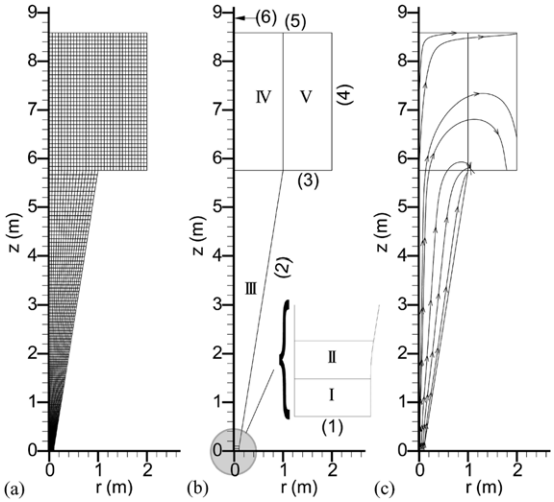

Figure 1. Magnetic nozzle geometry showing (*a*) computational mesh, (*b*) computational block structure with blocks and boundaries labelled and (*c*) initial magnetic field topology. Boundaries (1), (2), (3)–(5) and (6) are the inlet, nozzle wall, exit and axis of symmetry, respectively. Plasma is fed through boundary (1) of block I. Blocks II and III are the expansion region of the nozzle. Blocks IV and V enable modelling of plasma plume expansion downstream of the nozzle.

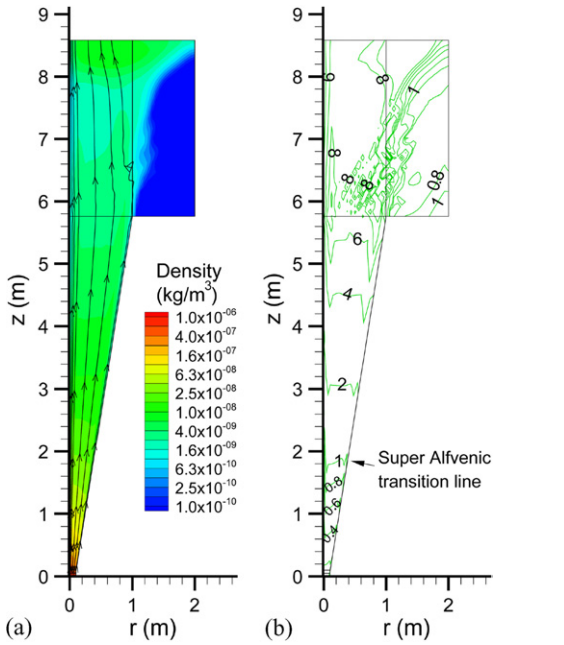

Figure 2. Magnetic nozzle modelling results using compatibility relations for (*a*) density and (*b*) Alfven Mach number contours at 4.5×10^{-4} s. Magnetic stream traces are shown in (*a*) for illustrative purposes.

above, $v_A \gg v_s$. The magnetic nozzle model, figure 1, was chosen with a modest expansion angle of 9° with a nozzle exit to inlet radius ratio of 10.0. The computational mesh, figure 1(*a*), consisted of 3328 grid cells, with 16 subdivisions along r for each block and 8, 8, 120, 36 and 36 for blocks I–V (figure 1(*b*)), respectively.

Following the guidelines of Arefiev and Breizman [2], the initial magnetic induction field lines are essentially straight inside the nozzle, figure 1(*c*). The field strength at the inlet was ∼0.25 T. The inlet conditions were determined as discussed above on boundary (1). The magnetic induction field was specified along the outer wall according to

$$B_{z,w} = \frac{B_{\mathrm{ref}} r_{\mathrm{ref}}^2}{r_w^2}, \qquad B_{r,w} = \tan(\alpha) B_{z,w}, \tag{13}$$

where the angle α is the nozzle wall angle, 9°. Boundaries (3)–(5) correspond to the exit across which both plasma and magnetic field are allowed to flow freely. Boundary (6) is an axis of symmetry. The inlet density and temperature for monatomic fully ionized hydrogen were $10^{21}\,\mathrm{m}^{-3}$ and 2 eV, respectively, which set the inlet Larmor radius and electron–ion mean free path of 10.0^{-3} m and 1.4×10^{-4} m, respectively. The axial (z) component of velocity was set to $10^4\,\mathrm{m\,s}^{-1}$. For these inlet conditions, equation (12) gives 8.81 as the minimum required radius ratio. We chose these conditions so that the plasma should just barely reach super-Alfvenic speed, so that effects from different inlet boundary conditions may be exaggerated.

The modelling was performed in two steps. Firstly, a steady state vacuum field was established using MACH2's magnetic field diffusion solver. The calculation was allowed to proceed until changes in values of test cells in the domain were less than $\sim 10^{-4}$%. Secondly, the flux was frozen into the domain by turning off the diffusion solver and allowing plasma to flow through the inlet. To avoid sharp discontinuities at the inlet, the density and velocity were ramped up to the intended value over 1 μs.

3.3. Description of boundary conditions to be compared

Three sets of boundary conditions were compared in order to evaluate the necessity of using the compatibility relations. In case 1, B_z is evaluated with equation (7), B_r is calculated with either equation (9) or (11), and v_r is calculated so the inlet flow is parallel to the magnetic induction field. In case 2, B_z, B_r and v_r are calculated using first order extrapolation from the computational domain. Finally, in case 3, B_z and B_r are 'frozen in' from the calculation of the vacuum field and v_r is set to 0.0.

4. Results

In the three cases studied, the inlet flow parameters and geometry are designed such that the plasma will transition from sub-Alfvenic to super-Alfvenic inside the computational domain. The initial vacuum field which curves radially outwards in blocks 4 and 5 should straighten as the super-Alfvenic plume expands downstream. We observed the expected behavior for both cases 1 and 2. Figures 2 and 3 show the density, magnetic field stream traces, and Alfven mach number contours at 4.5×10^{-4} s for cases 1 and 2. For case 1, the plasma has straightened the field lines, and smoothly transitions to super-Alfvenic speeds as shown. Case 2 gives similar results, although the magnetic field lines show some destabilization in the model by that time.

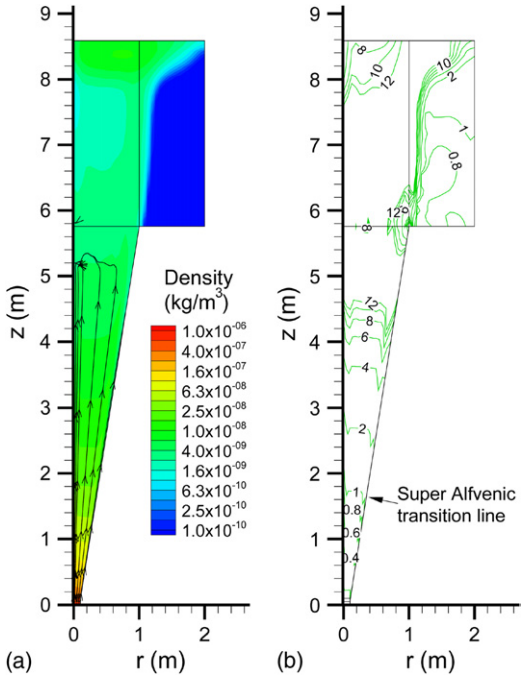

Figure 3. Magnetic nozzle modelling results using first order extrapolation for boundary conditions for (*a*) density and (*b*) Alfven Mach number contours at 4.5×10^{-4} s. Magnetic stream traces are shown in (*a*) for illustrative purposes.

While we can gain some physical insights from the numerical results, the real goal is to make a simple assessment of whether or not the implementation of the computational boundary conditions is successful. Numerical results indicate that the computed boundary conditions (cases 1 and 2) are stable to small perturbations, as the model persists until the plasma plume reaches the nozzle exit, around 4.5×10^{-4} s. Case 3, with all parameters specified, is unstable and crashes at 2.6×10^{-5} s. In both cases 1 and 2, the model crashes before 1 ms. The conditions downstream cause the magnetic induction field in the plume to behave erratically, with large disturbances eventually propagating upstream to the inlet and causing the model to crash. It is not clear at this time what leads to this behaviour.

A full assessment of the merits of the computational boundary conditions given in the appendix A requires verification of a test suite, such as the procedure discussed by Stone *et al* [12], and validation against experimental data if available. Nevertheless, we have noted that the computational boundary conditions (case 1) gave results consistent with the extrapolation method (case 2). Results from cases 1 and 2 gave qualitative results as expected. The computational boundary conditions made the numerical model marginally more stable than those using extrapolation. Hard coding the boundary conditions caused the numerical model to crash, verifying that some flow properties must be computed based on interior conditions when some of the characteristic waves point out of the domain.

5. Conclusion

We derived the compatibility equations using the method of projected characteristics for axisymmetric MHD flows. We simplified the expressions and developed an algorithm for including the boundary conditions in a numerical code. We ran some test cases to compare the use of boundary conditions derived from the compatibility relations, first order extrapolation and specification of all parameters at the boundary. These preliminary results suggest that computational boundary conditions are necessary for sub-Alfvenic inlet flows, either using the partial differential equations or extrapolation. The compatibility relations are slightly more stable than first order extrapolation. More tests will have to be done to thoroughly assess the accuracy and stability.

Acknowledgments

This effort was funded in part under NASA Contract NNJ05HB77C and by the Propulsion Research Center at the University of Alabama in Huntsville. The authors would like to thank Mr Michael Shreeves and Mr Ross Cortez for their assistance in preparation of this paper.

Appendix A. Method of projected characteristics for axisymmetric MHD flows

In a system of cylindrical coordinates (r, θ, z), the 2-temperature, inviscid, axisymmetric MHD equations of motion are:

Continuity

$$\frac{\partial \rho}{\partial t} + \frac{1}{r}\frac{\partial (r\rho v_r)}{\partial r} + \frac{\partial (\rho v_z)}{\partial z} = 0. \tag{A.1}$$

Momentum

$$\begin{aligned}
&\frac{\partial v_r}{\partial t} + v_r\frac{\partial v_r}{\partial r} + v_z\frac{\partial v_r}{\partial z} \\
&\quad + \frac{1}{\rho}\left\{\frac{\partial P}{\partial r} - \frac{1}{\mu_0}\left[B_z\left(\frac{\partial B_r}{\partial z} - \frac{\partial B_z}{\partial r}\right) - \frac{B_\theta^2}{r} - B_\theta\frac{\partial B_\theta}{\partial r}\right]\right\} = 0, \\
&\frac{\partial v_\theta}{\partial t} + v_r\frac{\partial v_\theta}{\partial r} + v_z\frac{\partial v_\theta}{\partial z} \\
&\quad - \frac{1}{\rho\mu_0}\left[B_r\left(\frac{B_\theta}{r} + \frac{\partial B_\theta}{\partial r}\right) + B_z\frac{\partial B_\theta}{\partial z}\right] = 0, \\
&\frac{\partial v_z}{\partial t} + v_r\frac{\partial v_z}{\partial r} + v_z\frac{\partial v_z}{\partial z} \\
&\quad + \frac{1}{\rho}\left\{\frac{\partial P}{\partial z} + \frac{1}{\mu_0}\left[B_\theta\frac{\partial B_\theta}{\partial z} + B_r\left(\frac{\partial B_r}{\partial z} - \frac{\partial B_z}{\partial r}\right)\right]\right\} = 0.
\end{aligned} \tag{A.2}$$

Electron energy

$$\begin{aligned}
&\frac{\partial \varepsilon_e}{\partial t} + v_r\frac{\partial \varepsilon_e}{\partial r} + v_z\frac{\partial \varepsilon_e}{\partial z} + \frac{P_e}{\rho}\left(\frac{1}{r}\frac{\partial (r v_r)}{\partial r} + \frac{\partial v_z}{\partial z}\right) \\
&\quad - \frac{\eta J^2}{\rho} + \frac{1}{\rho q_e n_e}\left(J_r\frac{\partial P_e}{\partial r} + J_z\frac{\partial P_e}{\partial z}\right) \\
&\quad - \frac{\kappa_\varepsilon}{\rho}\left[\frac{1}{r}\frac{\partial}{\partial r}\left(r\frac{\partial T_e}{\partial r}\right) + \frac{\partial^2 T_e}{\partial z^2}\right] \\
&\quad + \frac{1}{\rho}\Phi_{eR} + c_{v_e}\frac{(T_e - T_i)}{\tau_{ei}} = 0.
\end{aligned} \tag{A.3}$$

Ion energy

$$\frac{\partial \varepsilon_i}{\partial t} + v_r \frac{\partial \varepsilon_i}{\partial r} + v_z \frac{\partial \varepsilon_i}{\partial z} + \frac{P_i}{\rho}\left(\frac{1}{r}\frac{\partial (r v_r)}{\partial r} + \frac{\partial v_z}{\partial z}\right) - \frac{\kappa_i}{\rho}\left[\frac{1}{r}\frac{\partial}{\partial r}\left(r\frac{\partial T_i}{\partial r}\right) + \frac{\partial^2 T_i}{\partial z^2}\right] - c_{v_i}\frac{(T_e - T_i)}{\tau_{ei}} = 0. \quad \text{(A.4)}$$

Magnetic induction

$$\begin{aligned}
&\frac{\partial B_r}{\partial t} - \frac{1}{r}\left[-r\frac{\partial}{\partial z}\left(u_z B_r - u_r B_z\right)\right] + \frac{\eta}{r}\left(-r\frac{\partial J_\theta}{\partial z}\right) \\
&\quad + \frac{1}{q_e r}\left[-r\frac{\partial}{\partial z}\left(\frac{J_z B_r - J_r B_z}{n_e}\right)\right] = 0, \\
&\frac{\partial B_\theta}{\partial t} - \left[\frac{\partial}{\partial z}\left(u_\theta B_z - u_z B_\theta\right) - \frac{\partial}{\partial r}\left(u_r B_\theta - u_\theta B_r\right)\right] \\
&\quad + \eta\left(\frac{\partial J_r}{\partial z} - \frac{\partial J_z}{\partial r}\right) + \frac{1}{q_e}\left[\frac{\partial}{\partial z}\left(\frac{J_\theta B_z - J_z B_\theta}{n_e}\right)\right. \\
&\quad \left. - \frac{\partial}{\partial r}\left(\frac{J_r B_\theta - J_\theta B_r}{n_e}\right)\right] \\
&\quad - \frac{1}{q_e}\left[\frac{\partial}{\partial z}\left(\frac{1}{n_e}\frac{\partial P_e}{\partial r}\right) - \frac{\partial}{\partial r}\left(\frac{1}{n_e}\frac{\partial P_e}{\partial z}\right)\right] = 0, \\
&\frac{\partial B_z}{\partial t} - \frac{1}{r}\left[\frac{\partial}{\partial r}\left(r u_z B_r - r u_r B_z\right)\right] + \frac{\eta}{r}\left(\frac{\partial (r J_\theta)}{\partial r}\right) \\
&\quad + \frac{1}{q_e r}\left[\frac{\partial}{\partial r}\left(\frac{r J_z B_r - r J_r B_z}{n_e}\right)\right] = 0. \qquad \text{(A.5)}
\end{aligned}$$

The system is closed with an equation of state and various transport models. To write compatibility equations, we must first get the equations in form

$$\frac{\partial \boldsymbol{W}}{\partial t} + \boldsymbol{A}\frac{\partial \boldsymbol{W}}{\partial r} + \boldsymbol{C}\frac{\partial \boldsymbol{W}}{\partial z} - \boldsymbol{S} = 0, \qquad \text{(A.6)}$$

where $\boldsymbol{W}$ is the primitive variable vector given by

$$\boldsymbol{W} = [\rho \quad v_r \quad v_\theta \quad v_z \quad T_e \quad T_i \quad B_r \quad B_\theta \quad B_z]^T \qquad \text{(A.7)}$$

and vector $\boldsymbol{S}$ contains the source terms. Note that the energy equations are rewritten in terms of the ion and electron temperatures to use the primitive variables $\boldsymbol{W}$ as shown above. To derive the compatibility equations in the (z, t) plane, equation (A.6) is rewritten in the form

$$\frac{\partial \boldsymbol{W}}{\partial t} - \boldsymbol{C}\frac{\partial \boldsymbol{W}}{\partial z} = -\boldsymbol{A}\frac{\partial \boldsymbol{W}}{\partial r} + \boldsymbol{S} = 0 \qquad \text{(A.8)}$$

and the characteristic curves are determined by finding the eigenvalues ($\lambda^{(j)}$) and corresponding bigg eigenvectors ($\boldsymbol{\xi}^{(j)}$) of matrix $\boldsymbol{C}$. The compatibility equations along the projected characteristics are obtained in the following form:

$$\xi^{(j)}\frac{\partial \boldsymbol{W}}{\partial t} = -\xi^{(j)}\left(\boldsymbol{A}\frac{\partial}{\partial r} + \lambda^{(j)}\frac{\partial}{\partial z}\right)\boldsymbol{W} + \xi^{(j)}\boldsymbol{S} = 0. \qquad \text{(A.9)}$$

The coefficients of matrices $\boldsymbol{A}$, $\boldsymbol{C}$ and $\boldsymbol{S}$ are:

$$\boldsymbol{A} = \begin{pmatrix}
v_r & \rho & 0 & 0 & 0 & 0 & 0 & 0 & 0 \\
\frac{(\gamma-1)}{\rho}(C_{ve}T_e + C_{vi}T_i) & v_r & 0 & 0 & (\gamma-1)C_{ve} & (\gamma-1)C_{vi} & 0 & \frac{B_\theta}{\rho\mu_0} & \frac{B_z}{\rho\mu_0} \\
0 & 0 & v_r & 0 & 0 & 0 & 0 & -\frac{B_r}{\rho\mu_0} & 0 \\
0 & 0 & 0 & v_r & 0 & 0 & 0 & 0 & -\frac{B_r}{\rho\mu_0} \\
0 & (\gamma-1)T_e & 0 & 0 & v_r & 0 & 0 & 0 & 0 \\
0 & (\gamma-1)T_i & 0 & 0 & 0 & v_r & 0 & 0 & 0 \\
0 & 0 & 0 & 0 & 0 & 0 & v_r & 0 & 0 \\
0 & B_\theta & -B_r & 0 & 0 & 0 & 0 & v_r & 0 \\
0 & B_z & 0 & -B_r & 0 & 0 & 0 & 0 & v_r
\end{pmatrix}, \qquad \text{(A.10)}$$

$$\boldsymbol{C} = \begin{pmatrix}
v_z & 0 & 0 & \rho & 0 & 0 & 0 & 0 & 0 \\
0 & v_z & 0 & 0 & 0 & 0 & -\frac{B_z}{\rho\mu_0} & 0 & 0 \\
0 & 0 & v_z & 0 & 0 & 0 & 0 & -\frac{B_z}{\rho\mu_0} & 0 \\
\frac{(\gamma-1)}{\rho}(C_{ve}T_e + C_{vi}T_i) & 0 & 0 & v_z & (\gamma-1)C_{ve} & (\gamma-1)C_{vi} & \frac{B_r}{\rho\mu_0} & \frac{B_\theta}{\rho\mu_0} & 0 \\
0 & 0 & 0 & (\gamma-1)T_e & v_z & 0 & 0 & 0 & 0 \\
0 & 0 & 0 & (\gamma-1)T_i & 0 & v_z & 0 & 0 & 0 \\
0 & -B_z & 0 & B_r & 0 & 0 & v_z & 0 & 0 \\
0 & 0 & -B_z & B_\theta & 0 & 0 & 0 & v_z & 0 \\
0 & 0 & 0 & 0 & 0 & 0 & 0 & 0 & v_z
\end{pmatrix}, \qquad \text{(A.11)}$$

Table 1. Eigenvalues (column 2) and corresponding left eigenvectors for the matrix $\boldsymbol{C}$ as given in equation (A.11).

j	$\lambda^{(j)}$	$\xi^{(j)}$								
1	v_z	a_e^2	0	0	0	$\dfrac{-R_e\gamma\rho}{(\gamma-1)}$	0	0	0	0
2	v_z	0	0	0	0	T_i	T_e	0	0	0
3	v_z	0	0	0	0	0	0	0	0	1
4	$v_z + v_{Az}$	0	B_zB_θ	$-B_zB_r$	0	0	0	$-B_\theta v_{Az}$	$B_r v_{Az}$	0
5	$v_z - v_{Az}$	0	$-B_zB_\theta$	B_zB_r	0	0	0	$-B_\theta v_{Az}$	$B_r v_{Az}$	0
6	$v_z + v_{fz}$	$\dfrac{-v_{fz}(v_{fz}^2 - v_A^2)}{\gamma}$	$\dfrac{B_zB_r}{\mu_0}$	$\dfrac{B_zB_\theta}{\mu_0}$	$-\rho(v_{fz}^2 - v_{Az}^2)$	$\dfrac{-\rho v_{fz}R_e(v_{fz}^2 - v_A^2)}{a^2}$	$\dfrac{-\rho v_{fz}R_i(v_{fz}^2 - v_A^2)}{a^2}$	$\dfrac{-B_r v_{fz}}{\mu_0}$	$\dfrac{-B_\theta v_{fz}}{\mu_0}$	0
7	$v_z - v_{fz}$	$\dfrac{v_{fz}(v_{fz}^2 - v_A^2)}{\gamma}$	$\dfrac{B_zB_r}{\mu_0}$	$\dfrac{B_zB_\theta}{\mu_0}$	$-\rho(v_{fz}^2 - v_{Az}^2)$	$\dfrac{\rho v_{fz}R_e(v_{fz}^2 - v_A^2)}{a^2}$	$\dfrac{\rho v_{fz}R_i(v_{fz}^2 - v_A^2)}{a^2}$	$\dfrac{B_r v_{fz}}{\mu_0}$	$\dfrac{B_\theta v_{fz}}{\mu_0}$	0
8	$v_z + v_{sz}$	$\dfrac{-v_{sz}(v_{sz}^2 - v_A^2)}{\gamma}$	$\dfrac{B_zB_r}{\mu_0}$	$\dfrac{B_zB_\theta}{\mu_0}$	$-\rho(v_{sz}^2 - v_{Az}^2)$	$\dfrac{-\rho v_{sz}R_e(v_{sz}^2 - v_A^2)}{a^2}$	$\dfrac{-\rho v_{sz}R_i(v_{sz}^2 - v_A^2)}{a^2}$	$\dfrac{-B_r v_{sz}}{\mu_0}$	$\dfrac{B_\theta v_{sz}}{\mu_0}$	0
9	$v_z - v_{sz}$	$\dfrac{v_{sz}(v_{sz}^2 - v_A^2)}{\gamma}$	$\dfrac{B_zB_r}{\mu_0}$	$\dfrac{B_zB_\theta}{\mu_0}$	$-\rho(v_{sz}^2 - v_{Az}^2)$	$\dfrac{\rho v_{sz}R_e(v_{sz}^2 - v_A^2)}{a^2}$	$\dfrac{\rho v_{sz}R_i(v_{sz}^2 - v_A^2)}{a^2}$	$\dfrac{-B_r v_{sz}}{\mu_0}$	$\dfrac{B_\theta v_{sz}}{\mu_0}$	0

$$
\boldsymbol{S} = \begin{pmatrix}
\dfrac{\rho v_r}{r} \\
\dfrac{B_\theta^2}{r\mu_0\rho} \\
\dfrac{-B_r B_\theta}{r\mu_0\rho} \\
0 \\
\begin{pmatrix}(\gamma-1)T_e\dfrac{v_r}{r} - \dfrac{\eta J^2}{\rho C_{ve}} + \dfrac{m_e}{\rho^2 q_e}\left[\dfrac{-(\gamma-1)}{\mu_0}\dfrac{\partial B_\theta}{\partial z}\dfrac{\partial(\rho T_e)}{\partial r} + \dfrac{(\gamma-1)}{\mu_0}\left(\dfrac{\partial B_\theta}{\partial r} + \dfrac{B_\theta}{r}\right)\dfrac{\partial(\rho T_e)}{\partial z}\right] \\ -\dfrac{\kappa_\varepsilon}{\rho C_{ve}}\left(\dfrac{1}{r}\dfrac{\partial T_e}{\partial r} + \dfrac{\partial^2 T_e}{\partial r^2} + \dfrac{\partial^2 T_e}{\partial z^2}\right) + \dfrac{1}{\rho C_{ve}}\Phi_{eR} + \dfrac{(T_e - T_i)}{\tau_{ei}}\end{pmatrix} \\
(\gamma-1)T_i\dfrac{v_r}{r} - \dfrac{\kappa_i}{C_{vi}\rho}\left(\dfrac{1}{r}\dfrac{\partial T_i}{\partial r} + \dfrac{\partial^2 T_i}{\partial r^2} + \dfrac{\partial^2 T_i}{\partial z^2}\right) - \dfrac{(T_e - T_i)}{\tau_{ei}} \\
\dfrac{u_r B_r}{r} - \eta\dfrac{\partial J_\theta}{\partial z} + \dfrac{m_e}{q_e\rho^2}(J_z B_r - J_r B_z)\dfrac{\partial\rho}{\partial z} - \dfrac{m_e}{q_e\rho}\dfrac{\partial}{\partial z}(J_z B_r - J_r B_z) \\
\begin{pmatrix}u_\theta\dfrac{B_r}{r} + \eta\left(\dfrac{\partial J_r}{\partial z} - \dfrac{\partial J_z}{\partial r}\right) + \dfrac{m_e}{q_e}\left[\dfrac{\partial}{\partial z}\left(\dfrac{J_\theta B_z - J_z B_\theta}{\rho}\right) - \dfrac{\partial}{\partial r}\left(\dfrac{J_r B_\theta - J_\theta B_r}{\rho}\right)\right] \\ -\dfrac{m_e}{q_e}\left[\dfrac{\partial}{\partial z}\left(\dfrac{1}{\rho}\dfrac{\partial P_e}{\partial r}\right) - \dfrac{\partial}{\partial r}\left(\dfrac{1}{\rho}\dfrac{\partial P_e}{\partial z}\right)\right]\end{pmatrix} \\
u_r\dfrac{B_z}{r} + \dfrac{\eta}{r}\dfrac{\partial(rJ_\theta)}{\partial r} + \dfrac{m_e}{q_e r}\dfrac{\partial}{\partial r}\left(\dfrac{r(J_z B_r - J_r B_z)}{\rho}\right)
\end{pmatrix}. \tag{A.12}
$$

The corresponding eigenvalues and left eigenvectors for $\boldsymbol{C}$ are summarized in table 1, with the fast and slow magnetosonic speeds in the z direction given by

$$
v_{f,s} = \tfrac{1}{2}\left(a^2 + v_A^2 \pm \sqrt{a^4 + 2a^2v_A^2 + v_A^4 - 4a^2v_{Az}^2}\right)^{1/2}, \tag{A.13}
$$

where

$$
a^2 = \gamma RT = \gamma(R_eT_e + R_iT_i) \tag{A.14}
$$

and

$$
v_A^2 = \frac{(B_r^2 + B_\theta^2 + B_z^2)}{\rho\mu_0}, \tag{A.15}
$$

where v_{Az} is the Alfven speed in the z direction.

For positive flow into the inlet, the only possible characteristics that can point out of the domain are $v_z - v_{fz}$, $v_z - v_{Az}$ and $v_z - v_{sz}$. These waves correspond to $\lambda^{(j)}$ and $\boldsymbol{\xi}^{(j)}$ where $j = 7$, 5 and 9, respectively, according to table 1. The compatibility equations can be written in the tensor form

$$
\xi_{ji}\frac{\partial W_i}{\partial t} = \left(\tilde{A}_{ji}\frac{\partial}{\partial r} + \tilde{C}_{ji}\frac{\partial}{\partial z}\right)W_i + \tilde{S}_j \tag{A.16}
$$

where $(\tilde{A}_{ji}, \tilde{C}_{ji}, \tilde{S}_j) = (-\xi^{(j)}\boldsymbol{A}, -\xi^{(j)}\lambda^{(j)}, \xi^{(j)}\boldsymbol{S})$, respectively, and i refers to columns 3–11 in table 1. The coefficients for $j = 7(\mathrm{d}z/\mathrm{d}t = v_z - v_{fz})$, $j = 5(\mathrm{d}z/\mathrm{d}t = v_z - v_{Az})$ and $j = 9(\mathrm{d}z/\mathrm{d}t = v_z - v_{sz})$, are given below, where we have neglected the resistive, Hall, thermal magnetic, thermal

conduction and radiation terms:

$$\tilde{A}_7 = \begin{bmatrix} \left(-\frac{v_{fz}v_r}{\gamma}(v_{fz}^2 - v_A^2) - \frac{B_z B_r}{\rho\mu_0}\frac{a^2}{\gamma}\right) \\ \left(-\rho v_{fz}(v_{fz}^2 - v_A^2) - \frac{B_z B_r}{\mu_0}v_r - v_{fz}\frac{B_\theta^2}{\mu_0}\right) \\ \left(-v_r\frac{B_z B_\theta}{\mu_0} + v_{fz}\frac{B_\theta B_r}{\mu_0}\right) \\ \rho(v_{fz}^2 - v_{Az}^2)v_r \\ \left(-C_{ve}(\gamma-1)\frac{B_z B_r}{\mu_0} - \frac{\rho v_{fz}v_r R_e}{a^2}(v_{fz}^2 - v_A^2)\right) \\ \left(-C_{vi}(\gamma-1)\frac{B_z B_r}{\mu_0} - \frac{\rho v_{fz}v_r R_i}{a^2}(v_{fz}^2 - v_A^2)\right) \\ \left(-\frac{B_z B_r}{\mu_0^2}\frac{(-B_r - B_\theta - B_z)}{\rho} - \frac{B_r}{\mu_0}v_{fz}v_r\right) \\ \left(\frac{B_z B_r^2}{\mu_0^2\rho} - \frac{B_\theta}{\mu_0}v_{fz}v_r\right) \\ \frac{B_z B_r^2}{\mu_0^2\rho} \end{bmatrix}^{\mathrm{T}}, \tag{A.17}$$

$$\tilde{C}_7 = \begin{bmatrix} -\frac{v_{fz}}{\gamma}(v_z - v_{fz})(v_{fz}^2 - v_A^2) \\ -(v_z - v_{fz})\frac{B_z B_r}{\mu_0} \\ -(v_z - v_{fz})\frac{B_z B_\theta}{\mu_0} \\ \rho(v_z - v_{fz})(v_{fz}^2 - v_{Az}^2) \\ -\frac{\rho v_{fz}R_e}{a^2}(v_z - v_{fz})(v_{fz}^2 - v_A^2) \\ -\frac{\rho v_{fz}R_i}{a^2}(v_z - v_{fz})(v_{fz}^2 - v_A^2) \\ -v_{fz}(v_z - v_{fz})\frac{B_r}{\mu_0} \\ -v_{fz}(v_z - v_{fz})\frac{B_\theta}{\mu_0} \\ 0 \end{bmatrix}^{\mathrm{T}}, \tag{A.18}$$

$$\tilde{S}_7 = -\frac{9v_{fz}}{r}\left(\frac{B_r^2 v_r}{\mu_0} + \frac{B_r B_\theta v_\theta}{\mu_0} + \frac{\rho v_r}{\gamma}(v_{fz}^2 - v_A^2)\right) - \frac{9\rho v_{fz}}{a^2}(v_{fz}^2 - v_A^2)\left((\gamma-1)\frac{v_r}{r}(R_e T_e + R_i T_i) + \frac{(T_e - T_i)}{\tau_{ei}}(R_e - R_i)\right), \tag{A.19}$$

$$\tilde{A}_5 = \begin{bmatrix} 0 \\ -B_z \\ 0 \\ B_r \\ 0 \\ 0 \\ 0 \\ 0 \\ -v \end{bmatrix}^{\mathrm{T}}, \tag{A.20}$$

$$\tilde{C}_5 = \begin{bmatrix} 0 \\ 0 \\ 0 \\ 0 \\ 0 \\ 0 \\ 0 \\ 0 \\ (v_{Az} - v_z) \end{bmatrix}^{\mathrm{T}}, \tag{A.21}$$

$$\tilde{S}_5 = -\frac{9v_r B_z}{r}, \tag{A.22}$$

$$\tilde{A}_9 = \begin{bmatrix} \left(-\frac{v_{sz}v_r}{\gamma}(v_{sz}^2 - v_A^2) - \frac{B_z B_r}{\rho\mu_0}\frac{a^2}{\gamma}\right) \\ \left(-\rho v_{sz}(v_{sz}^2 - v_A^2) - \frac{B_z B_r v_r}{\mu_0} - v_{sz}\frac{B_\theta^2}{\mu_0}\right) \\ 0 \\ \left(-v_r\frac{B_z B_\theta}{\mu_0} + v_{sz}\frac{B_\theta B_r}{\mu_0}\right)\frac{\partial v_\theta}{\partial r} + \rho v_r(v_{sz}^2 - v_{Az}^2) \\ \left(-C_{ve}(\gamma-1)\frac{B_z B_r}{\mu_0} - \frac{\rho v_r v_{sz}R_e}{a^2}(v_{sz}^2 - v_A^2)\right) \\ \left(-C_{vi}(\gamma-1)\frac{B_z B_r}{\mu_0} - \frac{\rho v_r v_{sz}R_i(v_{sz}^2 - v_A^2)}{a^2}\right) \\ \left(-\frac{B_z B_r(-B_r - B_\theta - B_z)}{\rho\mu_0^2} - v_{sz}v_r\frac{B_r}{\mu_0}\right) \\ \left(\frac{B_z B_r^2}{\mu_0^2\rho} - v_{sz}v_r\frac{B_\theta}{\mu_0}\right) \\ \frac{B_z B_r^2}{\mu_0^2\rho} \end{bmatrix}^{\mathrm{T}}, \tag{A.23}$$

$$\tilde{C}_9 = \begin{bmatrix} -\frac{v_{sz}}{\gamma}(v_z - v_{sz})(v_{sz}^2 - v_A^2) \\ -(v_z - v_{sz})\frac{B_z B_r}{\mu_0} \\ -(v_z - v_{sz})\frac{B_z B_\theta}{\mu_0} \\ \rho(v_z - v_{sz})(v_{sz}^2 - v_{Az}^2) \\ -\frac{\rho v_{sz}R_e}{a^2}(v_z - v_{sz})(v_{sz}^2 - v_A^2) \\ -\frac{\rho v_{sz}R_i}{a^2}(v_z - v_{sz})(v_{sz}^2 - v_A^2) \\ -v_{sz}(v_z - v_{sz})\frac{B_r}{\mu_0} \\ -v_{sz}(v_z - v_{sz})\frac{B_\theta}{\mu_0} \\ 0 \end{bmatrix}^{\mathrm{T}}, \tag{A.24}$$

$$\tilde{S}_9 = -\frac{9v_{sz}}{r}\left(\frac{B_r^2 v_r}{\mu_0} + \frac{B_r B_\theta v_\theta}{\mu_0} + \frac{\rho v_r}{\gamma}(v_{sz}^2 - v_A^2)\right) - \frac{9\rho v_{sz}}{a^2}(v_{sz}^2 - v_A^2)\left(\frac{(\gamma-1)v_r}{r}(R_e T_e + R_i T_i) + \frac{(T_e - T_i)}{\tau_{ei}}(R_e - R_i)\right). \tag{A.25}$$

References

[1] Arefiev A V and Breizman B N 2004 Theoretical components of the VASIMR plasma propulsion concept *Phys. Plasmas* **11** 2942–9

[2] Arefiev A V and Breizman B N 2005 Magnetohydrodynamic scenario of plasma detachment in a magnetic nozzle *Phys. Plasmas* **12** 043504

[3] Kaufman D A, Goodwin D G and Sercel J C 1993 Plasma separation from magnetic field lines in a magnetic nozzle *31st Aerospace Sciences Meeting and Exhibit* (*Reno, NV, 11–14 January 1993*)

[4] Hooper E B 1993 Plasma detachment from a magnetic nozzle *J. Propulsion and Power* **9** 757–63

[5] Ilin A V, Diaz F R C, Squire J P, Tarditi A G, Breizman B N and Carter M D 2002 Simulations of plasma detachment in VASIMR *40th AIAA Aerospace Sciences Meeting and Exhibit* (*Reno, Nv, 14–17 January 2002*)

[6] York T M, Jacoby B A and Mikellides P G 1992 Plasma flow processes within magnetic nozzle configurations *J. Propulsion Power* **8** 1023–30

[7] Nakagawa Y 1981 Evolution of magnetic field and atmospheric response: I. Three-dimensional formulation by the method of projected characteristics *Astrophys. J.* **15** 247 707–18

[8] Nakagawa Y, Hu Y Q and Wu S T 1987 The method of projected characteristics for the evolution of magnetic arches *Astron. Astrophys.* **179** 354–70

[9] Wu S T and Wang J F 1987 Numerical tests of a modified full implicit continuous Eulerian (FICE) scheme with projected normal characteristic boundary conditions for MHD flows *Comput. Methods Appl. Mech. Eng.* **64** 267–82

[10] Peterkin R E J, Frese M H and Sovinec C R 1998 Transport of magnetic flux in an arbitrary coordinate ALE code *J. Comput. Phys.* **140** 148–71

[11] Peterkin R E J and Frese M H 1998 *MACH: A Reference Manual* 1st edn (Air Force Research Laboratory, Phillips Research Site)

[12] Stone J M, Hawley J F, Evans C R and Norman M L 1992 A test suite for magnetohydrodynamical simulations *Astrophys. J.* **388** 415–37